This is an Accepted Manuscript of an article published by Taylor & Francis Group in MARINE GEODESY on 11/10/2017, available online: https://doi.org/10.1080/01490419.2017.1373173

Three-Dimensional Geographically Weighted Inverse Regression (3GWR) Model for Satellite Derived Bathymetry Using Sentinel-2 Observations

Andrzej Chybicki

Department of Geoinformatics, Electronics, Telecommunications and Informatics Faculty, Gdańsk University of Technology, Gdańsk, Poland

ABSTRACT

Current trends of development of satellite derived bathymetry (SDB) models rely on applying calibration techniques including analytical approaches, neuro-fuzzy systems, regression optimization and others. In most of the cases, the SDB models are calibrated and verified for test sites, that provide favorable conditions for the remote derivation of bathymetry such as high water clarity, homogenous bottom type, low amount of sediment in the water and other factors. In this paper, a novel 3-dimensional geographical weighted regression (3GWR) SDB technique is presented, it binds together methods already presented in other studies, the geographically weighted local regression (GWR) model, with depth dependent inverse optimization. The proposed SDB model was calibrated and verified on a relatively difficult test site of the South Baltic near-shore areas with the use of multispectral observations acquired by a recently launched Sentinel-2 satellite observation system. By conducted experiments, it was shown that the proposed SDB model is capable of obtaining satisfactory results of RMSE ranging from 0.88 to 1.23[m] depending on the observation and can derive bathymetry for depths up to 12m. It was also shown, that the proposed approach may be used operationally, for instance, in the continuous assessment of temporal bathymetry changes, for areas important in the context of ensuring local maritime safety.

KEYWORDS Bathymetry; Baltic; derived; local; multispectral; observation; regression; remote; satellite; Sentinel; weighted

Introduction

SDB is one of the key tools that allows for the provision of worldwide shallow water monitoring capabilities at a relatively low cost. Current trends in the development of SDB methods rely on the application of optimization techniques for a set of calibrating points in order to obtain a relatively precise model of water depths in near shore areas (Lyzenga 1981; Ma et al. 2014; Lafon et al. 2002). High accuracy SDB models have a significant influence in many fields of engineering as they allow for the mapping of bathymetry changes in near-shore areas and support the safety of shallow water maritime routes in critical locations

(Pe'eri et al. 2014; Moszynski et al. 2015). The precise methods of the remote mapping of bathymetry are also of high importance for many fields of geosciences (Kulawiak et al. 2010) (Pacheco et al. 2015; Forfinski-Sarkozi and Parrish 2016), for instance, in environmental studies, where remotely estimated bathymetry helps to generate a better understanding of environmental phenomena, such as water sediment monitoring (Wieczorek et al. 2014), temporal changes in water quality (Doernhoefer et al. 2016, 2), coral reef cover observations (Hamylton et al. 2015), marine archaeology (Guzinski et al. 2016) or glacial lake changes (Moussavi et al. 2016; Pope et al. 2016).

Currently, SDB studies are focused on enhancing empirical model performance by utilizing various optimization techniques such as global and local regression models (Su et al. 2014), artificial networks (Jena et al. 2012), fuzzy models (Kobryn et al. 2013; Corucci et al. 2011; Mishra et al. 2007) and analytical approaches (Brando and Dekker 2003) (Hoge and Lyon 1996; Lee et al. 1998). So far, most of the optimization techniques in this field were applied to geographical test sites in areas that provide favorable conditions to derive bathymetry from remote observations (Table 1.). However, there are several studies related to the investigation of this issue in more demanding, optically complex waters, for instance, in the Baltic Sea (Vahtmaee and Kutser 2016; Vahtmäe et al. 2006) or Singapore (Bramante et al. 2013). Significant improvements to this field of science were also brought about by applying physical modelling to the process of bathymetry estimation. This was achieved by utilizing

Table 1. Comparison of basic features of selected SDB models.

Author(s)/ publication year	RMSE [m]	Satellite sensor/ spatial resolution [m]	Location(s)	Max. derivation depth [m]	Remarks
(Lyzenga et al. 2006)	1.74 – 3.02	IKONOS/3.2	Cancun, Duck NC, Kahana Bay, Carysoft Reef FL, Pearl Harbour, HI Diamond Head HI, Maunaloa Bay, HI	16–24 (depending on location)	
(Stumpf et al. 2003)	0.2–0.7	IKONS/3.2 Landsat 7/30	Kure Atoll – Hawaiian Islands,	25–30	
(Ma et al. 2014)	0.62–1.73	Hyperion/30	O'Ahu Island, Saint Thomas Island	25	RMSE 2.57–3.35 [m] for depths > 25m
(Su et al. 2008)	1.25 (local models) 2.34 (global approach)	Landsat 7/30	Kauai Island, Barbuda Island, HI,	17–18	
(Vinayaraj et al. 2016)	1.7–1.82 (for local approach) 2.48–2.63 for global models	Landsat 8/30 RapidEye/5	South-Eastern coast of Puerto Rico	20	
(Mishra et al. 2006)	1.316–2.819	QuickBird/2.4	Routan Island, Honduras	18–35	
(Mishra et al. 2005)	2.711	IKONOS/3.2	West coast, Honduras	>40	
(Hamylton et al. 2015)	N/A	WorldView-2/0.5	Lizard Island, Australia Sykes Reef, Australia	27 – 30	Residual values (difference between model and estimated depths) in most of cases was in range between −10.4 to 5 [m]
(Eugenio et al. 2015)	1.2–1.94	WorldView-2/0.5	Canary Islands	25–35	Correlation coefficient 0.93–0.94

radiative transfer models in order to account for the existence of optically active constituents of the water column (Spitzer and Dirks 1986; Mobley et al. 2005; Brando et al. 2009; Giardino et al. 2012; Pope and Fry 1997).

Generally, to date the most promising results have been obtained for test sites that are characterized by low amounts of sediment in the water, a homogenous bottom type and a small spatial diversity of water quality, i.e. the Florida coast (Lyzenga et al. 2006), Hawaiian Islands (Stumpf et al. 2003), Caribbean (Ma et al. 2014) , the Australian coast (Hamylton et al. 2015) or the west coast of Roatan Island, Honduras (Mishra et al. 2005). In such cases, the appropriate model of calibration allows for the derivation of water depths even for points located up to 30 m under water surface thus obtaining the RMSE below 2.5 m. Applying local regression models, though harder to implement, can reduce the RMSE error to just a 1m range. Model quality can be also be enhanced by using more precise observation instruments (increased spatial, radiometrical and quantization resolution) for instance, from newly available satellite systems such as Landsat 8, Hyperion or commercial systems such as IKONOS, QuickBird or WorldView-2 (Lee et al. 2012). In this case, more information about the observed area is delivered to the model and therefore its general performance may be increased. Particularly for high resolution observations, approaches that focus on atmospheric and sunglint data correction are of high importance as proper data pre-processing enables for taking advantages from higher quality of observations (Eugenio et al. 2015; Mahiny and Turner 2007; Chavez et al. 1996).

The presented studies above indicate the high degree of usefulness of SDB, however, at least three important issues have not been addressed in sufficient detail to date. Firstly, not much attention is being paid to more problematic sites in order to analyze whether freely available remote observations may be useful in other climatic regions/zones. Secondly, the opportunities presented by the recently launched ESA Senitnel-2 (S2) system, which has been assigned the task of observing the European continent, hasn't been sufficiently utilized in the context of SDB (Hedley et al. 2012). Thirdly, and possibly most important point, how current methods of SDB may be improved in order to achieve a higher level of precision, specifically for more demanding test cases.

Therefore, in this paper, the problem of SDB retrieval for the region of the South Baltic coast was addressed. The author proposes the novel concept of a 3-dimensional locally weighted geographical regression (3GWR) which relies on applying local regression not only in the planar (geographical) plane (as it was presented in previous studies)(Su et al. 2014; Su et al. 2015), but also in the vertical (depth related) plane of the analyzed region. The proposed model was calibrated and verified on the basis of observations acquired from the European Space Agency Senitnel-2 satellite system.

Methods

Satellite derived bathymetry is generated from remote multispectral observations obtained from visible bands of electromagnetic spectra with the use of additional information required for accurate model calibration (Knudby et al. 2016; Vinayaraj et al. 2015; Lyzenga 1977). Currently, no predefined set of model parameters is available, therefore every model requires a set of training points, where the exact location, connected to the *a priori* known depths, is required, in order to best fit (usually in terms of LSE) the SDB observation estimator to in-situ measured bathymetry. The bathymetry is usually acquired by single beam

echosounder (SBE), mutlibeam sonars (MBS) or is derived indirectly by the LiDaR system. Other forms of retrieving calibration data include methods of bathymetry retrieval from ENC, nautical charts or external marine data sources.

The overall concept of the SDB retrieval model relies on the physical phenomena of light attenuation in the water column and it's reflection from the bottom to a certain depth. The level of backscattered light registered at the satellite sensor is generally inversely proportional to the depth of the observed pixels on the water surface. In order to maximize the depths that can be derived by satellite measurements, bands with the lowest level of light absorption in water are used: mainly blue and green. However, in case of hyperspectral sensors (i.e. Hyperion), the number of usable bands may be higher (Liu 2013).

Satellite bathymetry derivation using global optimization

The main principle of SDB models relies on the phenomena of light passing through a water column of a certain depth described by the Beer-Lambert law (Eq. 1)

$$I = I_0 \, e^{-kz}, \tag{1}$$

which connects the portion of light energy before (I_0) and after (I) passing through the water column of a certain depth z, and light attenuation coefficient k. When deriving the bathymetry from a multispectral sensor, energy is registered in various wavelengths as it is attenuated by the water in different degrees. Using regression or approximation techniques of light reflected from the bottom, the water depth of observed pixels can be estimated. The basic SDB retrieval model constitutes four basic components, namely:

- light absorption in the atmosphere which, in most cases, is assumed to be constant over an area or it's effect is removed during satellite data processing,
- water surface optical effects related to light reflection,
- light attenuation in the water column during its passage on the pathway from the water surface to the bottom and back,
- bottom reflectance of light for optically shallow water – this component is apparent only when the light of certain wavelengths reaches the bottom.

In order to maximize the depths that can be estimated on the basis of the model, most techniques utilize passive optical scanners of wavelengths that have the smallest possible water attenuation coefficients. For instance, sunlight in the blue band (450–495 nm), in favorable conditions, can even reach 30 m depths, while green light (495–570 nm) usually penetrates water to depths less than 15 m (Allen et al. 2017) (Luchinin and Kirillin 2016).

One of the main satellite derived bathymetry approaches, originally proposed by Stumpf (Stumpf et al. 2003), uses the log-ratio technique to obtain the spatial distribution (map) of the SDB estimator obtained from remote observation. This model assumes that as the water depth increases, reflectance values in the band characterized by higher levels of absorption will decrease faster than those with a lower level of absorption. Moreover, this empirical approach implicitly accounts for the change in bottom albedo as bottom type heterogeneity which affects both bands in a similar way, while changes in depth are directly observed. At the first step of this process, the estimator is computed as the ratio of logarithms of selected

optical bands for points located at position (x, y) :

$$z_{est}(\mathrm{x},\mathrm{y}) \ = \alpha_0 \ + \alpha_1 \frac{\ln(R(\chi_b(\mathrm{x},\mathrm{y})))}{\ln\left(R\left(\chi_g(\mathrm{x},\mathrm{y})\right)\right)}, \tag{2}$$

where α_0 and α_1 are coefficients of the model to be optimized during model calibration and are set with initial values (for instance 0 and 1 respectively) before model calibration, $R(\lambda_b(x, y))$ and $R\left(\lambda_g(x, y)\right)$ are corrected remote sensing radiances for optical bands λ_b and λ_q (i. e. blue and green respectively).

In order to properly calibrate the model, for instance, in the sense of least squared distance (LSE), iterative or analytic fitting is used. It relies on finding the estimated value for which the global cost function J_G reaches a minimum:

$$J_G = \ E\left[\frac{1}{2}\sum_{i=1}^{n}(z_i - \hat{z}_i)^2\right] = \ E\left[\frac{1}{2}\sum_{i=1}^{n}\left(z_i - \emptyset(o_i)^{\mathrm{T}}\alpha\right)^2\right], \tag{3}$$

where $E[\cdot]$ is an expected value operator, n is the number of training points, i is the observation number, z_i is the depth of the *i-th* calibration point, $\hat{z}_i$ is the model value which can be expanded as a basis function of observations o_i – vector $\emptyset\left(\wr\right)^{\mathcal{T}}$. In general, the solution to the optimization problem defined in Eq. 2 is the $\hat{\alpha}$ vector of (linear) regression coefficients:

$$\hat{\alpha} = [X^T W X]^{-1} \ X^T W z \tag{4}$$

where each row of $X \in \mathbb{R}^{n\times m}$ contains m training data coefficients for the i-th observation, $W \in \mathbb{R}^{n\times n}$ is the optional matrix, where diagonal entries represent the importance of the i-th observation and z is the column vector constructed from z_i values.

The main advantage of this approach is that it is relatively robust and does not require either high computational power or auxiliary information to set the model parameters optimally if the calibration points are calculated accurately. The model, in this form, can be used at all scales, however, when dealing with larger areas, the results are usually worse as the global approach is not capable being fit to local distortions of environmental parameters like water turbidity, bottom type variety and other factors. (Cleveland and Devlin 1988).

Geographical weighted local regression model – GWR

In contrast to global approach learning systems, local optimization models split up the global problem into multiple simpler learning problems (Stulp and Sigaud 2015). Traditional geographically weighted regression (GWR) (Fotheringham et al. 1998) approaches achieve this by dividing up the global cost function $J_G^{'}$ into a sum of multiple independent local cost functions:

$$J_G^{'} = \ E\left[\frac{1}{2}\sum_{l=1}^{L}\sum_{i=1}^{N}\left[w_{l,i}\left(z_i - \emptyset(o_i)^{\mathrm{T}}\alpha_{\mathrm{k}}\right)^2\right]\right] = \sum_{l=1}^{L} E\left[\frac{1}{2}\sum_{i=1}^{n} w_{l,i}\left(z_i - \emptyset(o_i)^{\mathrm{T}}\alpha_{\mathrm{k}}\right)^2\right] = \frac{1}{2}\sum_{l=1}^{L} J_l \tag{5}$$

where $w_{l,i}$ is the weight of the i-th observation in l-th ($l = (1, 2, \ldots, L)$) local model. This approach is particularly useful, when the optimization of the model concerns observations that are locally dependent (Kanno et al. 2011). In such cases, local regression models are usually capable of increasing overall model quality.

In the locally optimized SDB model, weighting windows, that define the geographical local sub-center of training dataset, must be defined *a priori*. Therefore, for every calibration point, the weighting kernel is centered at the local model midpoint, and the further the distance from the local model center, the more the importance of calibration for a particular point decreases.

In the local approach, the SDB model from Eq. 2 can be rewritten using the local dependence of model parameters as follows:

$$z(x,y) = \alpha_0 (x,y) + \sum_j \alpha_j(x,y)\hat{B}(x,y) \tag{6}$$

where $\hat{B}(x,y)$ is the local SDB estimator derived from initial conditions from Eq. 2. and j is the number of selected spectral components of remote observations.

In order to account for the locality of $\alpha_j(x,y)$ parameters ($j = (0, 1, \ldots)$), the spatial weights are set during local model calibration. For GWR, the 2D weights of the l-th local model for point located at (x,y) are usually computed with the use of the inverse distant function:

$$w_l (x,y) = \left[1 - \left(\frac{\mathrm{d_l}}{\mathrm{b}} \right)^2 \right]^2 , \text{if } \mathrm{d_l} < \mathrm{b} , \tag{7}$$

and

$$w_l (x,y) = 0 \text{ else}, \tag{8}$$

where d_l is the distance of the point, located at position x, y, to the l-th local model window center and b is the geographical window width (usually equal for all local models). The proper selection of window width and local center localization is important because the wider the windows, the smoother the results of the model which are obtained. On the other hand, the wide windows of the local model make the regression less sensitive to local conditions of function to be locally approximated.

The solution to the GWR approach, specified in Eqs. 5–8, is analogous to the global approach, however in this case, W_l applies only to the l-th local model parameters to be fitted in order to minimize local cost functions:

$$\hat{\alpha}_l = [X^T W_l X]^{-1} X^T W_l z \tag{9}$$

where $W_l \in \mathbb{R}^{n \times n}$ is the optional matrix, where diagonal entries represent the importance of the i-th observation proportional to its distance from the model center (Eqs. 7 and 8)

Local inverse optimization width depth windowing – 3GWR

As presented above, GWR models can be effectively fit to the geographically spread heterogeneity of the function to be estimated. However, when estimating bathymetry from

spaceborne optical sensors, not only geographical variety of phenomena is important but also the issue of depth dependency of model parameters should be considered in order to obtain the best possible estimation (Kyriakidis et al. 2016). Therefore, in this paper, a 3-dimensional geographically weighted regression model (3GWR) which is an expansion of the GWR model functionality, is presented. The proposed approach is novel, because it introduces another set of local models, coupled with a particular local GWR model, determined by the depth of the pixels to be estimated. This is achieved by applying a two-step procedure in the process of determining the pixel depth. In first step, the depth is determined on the basis of locally adjusted depth dependent models. Next, the final depth of the pixel is calculated as a weighted average of locally depth dependent estimations. This means that the local regression coefficients do not only depend on the geographical position of the point to be estimated, as in GWR model, but also on its depth.

In this case, the cost function of the set of local problems is formulated as:

$$J_G^{'\prime} = E\left[\frac{1}{2}\sum_{l=1}^{L}\sum_{d=1}^{D}\sum_{i=1}^{N}\left[w_{l,i}\ w_{l,d,i}\left(z_i - \emptyset(o_i)^{\mathrm{T}}\alpha_{\mathrm{d}}\right)^2\right]\right] = \frac{1}{2}\sum_{l=1}^{L}\sum_{d=1}^{D} J_{d,l} \tag{10}$$

where D is the total number of depth-dependent local models, $d = (1, 2, ..D)$. In this case, finding an estimation $\hat{\alpha}_D$, for which $J_G^{'\prime}$ is minimal, requires constructing an additional set of constraint matrix equations, this is analogous to the GWR approach, that accounts for the heterogeneity of the model in depth plane. In this case the local model determined by depth parameters $\hat{\alpha}_D$ are determined by the following equation:

$$\hat{\alpha}_d = \left[X^T W_d X\right]^{-1} X^T W_d z \tag{11}$$

where W_d is a depth dependent weight matrix for center depth d, where diagonal entries represent the weight inversely proportional to the distance from the d-th depth-dependent local sub-model center.

The combination of the set of geographically and depth dependent models allows the spatially continuous SDB coverage product (map) to be obtained and is performed with the use of a two-step procedure (Figure 1). Firstly, the initial SDB estimator $\hat{B}(x, y)$ taken from the initial conditions of Eq. 2 is calculated for the pixel located at (x, y). Then, the depths $z_1(x, y)$, ..., $z_D(x, y)$ are determined by D depth dependent models (denoted as $DM_1, .., DM_D$). Then, each local (in the sense of depth dependency) depth $z_i(x, y)$, ($i = (1, 2, \ldots D)$), is weighted using inverse distant weights $w_1, \ldots, w_D$. The resulting local depth dependent value $Z(x, y)$, is then processed by a standard GWR scheme (step 2), where $LM_1, .., LM_L$ denote local GWR models and $W_1(x, y), \ldots, W_L(X, y)$ are geographically (inverse distant) determined weights.

Materials

Remote observation from Sentinel-2 system

In the study, four images of the Gdańsk Gulf and part of the south coast of the Baltic, registered in spring of 2016, were acquired in order to evaluate the proposed approach. Namely, 4 observations from this period acquired on 4th March 2016, 9th March 2016, 27th March

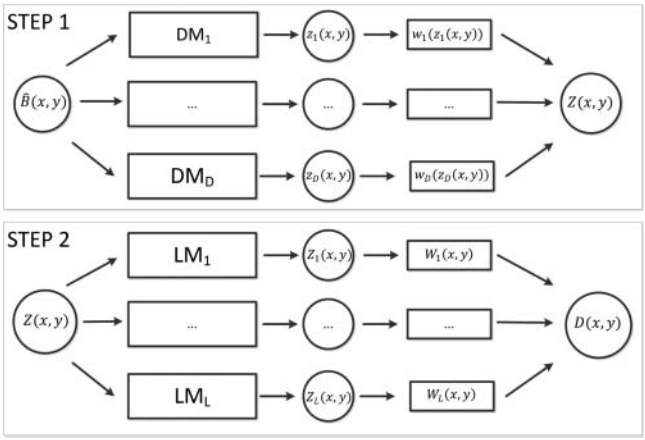

Figure 1. Scheme of 3GWR method – two-step procedure for creating a continous map of SDB using the proposed approach.

2016 and 6th May 2016 were extracted. Note that, these are one of the first acquisitions of the Sentinel-2 system available. At the time this study was performed, only one of the two planned Sentinel-2 satellites, was fully operational in orbit (Sentinel-2A). Therefore, the revisit time was longer than it was or the full constellation and thus the number of available acquisitions made under clear sky conditions was smaller.

Sentinel-2 is the polar orbiting satellite system that provides high-resolution multispectral observations of land and sea. S2, as a part of the ESA Copernicus Programme, which is dedicated to providing observational data to European users, however, global observations are available in a 2–5 day (depending on the latitude) repeat cycle. The Multispectral Instrument (MSI) sensor, mounted on the Sentinel-2 satellite, registers observed radiation in 12 bands, ranging from the optical 443 nm (±10 nm) to near infrared (NIR) 2190 nm (±90 nm). The spatial resolution of the observations depends on the registered wavelength and ranges from 10 m. to 60 m. For the purposes of this research, two optical bands, blue (490 nm ± 32 nm) and green (560 nm ± 17 nm), that provide observations in a $10\,m \times 10\,m$ regular UTM 34N cartographic grid, were used for the calibration of the proposed 3GWR algorithm.

Data from S2 is provided to scientific users via the SciHub portal which is dedicated to the ESA mirror site for providing Copernicus data. The SciHub portal allows for browsing, filtering and downloading necessary observations and meta data provided in a Level 1C stage product composed of 100 × 100 km^2 tiles (ortho-images in UTM/WGS84 projection) in top of the atmosphere (TOA) reflectance. Since the S2 mission is land-oriented no predefined scheme for providing atmosphere corrected reflectance over water surfaces is available (Toming et al. 2016). Although there are several atmosphere dedicated correction schemes (sen2cor, ACOLITE) for water reflectance determination using MSI (Martins et al. 2017; Doernhoefer et al. 2016), their implementation is not trivial, and usually requires high resolution transmittance data or aerosol spatial distribution to be provided. However, since the proposed methodology is based on the local empirical modelling approach and due to the fact that aerosol dispersion varies in scales of kilometers (Kay et al. 2009), the simplified Gauss averaging filter of L1A data was applied in order to account for sun glint and specular effects. In this case, applying more sophisticated schemes, such as utilizing NIR data (Harborne and Mumby 2005), didn't produce a significant improvement in the model performance.

In order to distinguish water reflectance pixels from land, a simple NIR thresholding method was applied. Cloud masking was performed on the basis of the provided L1C data vector mask in the GML format.

Model calibration and validation

Model calibration and validation was performed with the use of single beam echosounder soundings acquired by the Polish Maritime Administration (PMA), which is an official domestic entity responsible for maritime safety and security, marine route monitoring and management for the spatial planning and environmental protection of the Polish Baltic economic zone. The PMA performs periodic surveys, with the use of echo sounding equipment in order to prepare data for official navigation charts produced by the Naval Hydrographical Office. The dataset for this study was acquired in the period between 2010 and 2015 and is constituted from several single beam echosounder profiles perpendicular to the coastline. The spacing between the profiles is around 500 m and, within each profile, the sounding spacing is about 10–15 m (Figure 2). Unfortunately, obtaining time co-incident echosounding datasets and remote observations was not possible for the time period in which the Sentinel-2 observations were acquired.

In order to evaluate the quality of the results obtained by the proposed SDB model, the iterative *leave-p-out cross-validation* scheme, was applied. The general outline of this scheme is based on the iterative repetition of the calibration and validation procedure of the model performed on randomly divided subdatasets. Namely, within each iteration, the input PMA dataset was randomly divided into two separate subsets: the training dataset (TD), used for the calibration of the algorithm, and the validation dataset (VD) used for the evaluation of obtained results (Figure 3).

Then, the results of each iteration were evaluated using two basic statistical factors, namely the sample correlation coefficient defined and calculated as:

$$R = \frac{\sum_{i=1}^{N}\left(\hat{d}_i - \overline{d}\right)\left(d_i - \overline{d}\right)}{\sqrt{\sum_{i=1}^{N}\left(\hat{d}_i - \overline{d}\right)^2}\sqrt{\sum_{i=1}^{N}\left(d_i - \overline{d}\right)^2}} \tag{12}$$

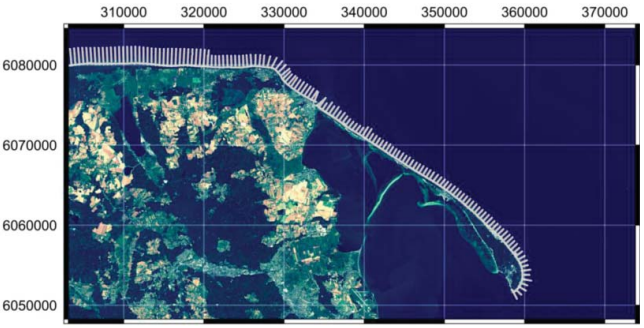

Figure 2. PMA sounding dataset points and test site used in the study. Grey marker lines, perpendicular to the coastline, represent the locations of soundings acquired by the PMA using an SBE echosounder. Coordinates are given in the original Sentinel-2 coordinate system – UTM 34N zone [meters].

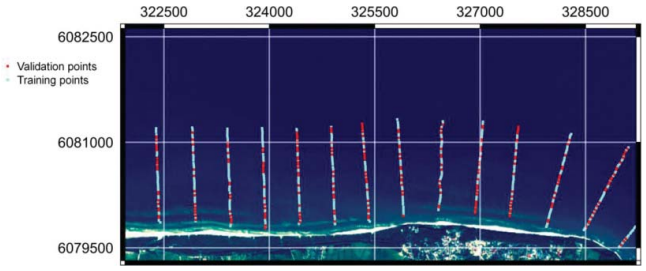

Figure 3. Detail view of the training data points and validation data for a location near Jastrzębia Góra city (54.832043° N, 18.307413° E).

where $\hat{\overline{d}}$ is the expected value (mean) of $SDB - \hat{d}$, and $\overline{d}$ is the expected value (mean) of d (depths from TD or VD respectively) and N is the number of elements in the tested population and root mean squared error (RMSE) defined as :

$$RMSE = \sqrt{\frac{\sum_{i=1}^{N}\left(\hat{d}_i - d_i\right)^2}{N}} \tag{13}$$

In order to verify whether the results in each iteration are representative, the statistics of TD and VD datasets obtained in each iteration are presented in the form of a global comparison in Table 2.

What is important to note is that, although in particular iterations of the validation scheme, datasets were divided randomly, the main statistical features between iterations were preserved. The normalized number of sounding points that fall within a particular depth range differs in each iteration, however, variations are usually less than 1%. For instance, in all iterations the number of points falling within the 4–6 [m] depth range,

Table 2. Test site calibration dataset – statistical description.

	Training dataset			Validation dataset		
Total no. of Points	2571			1071		
Date of acquisition	2010–2015					
Bounds [m] in UTM 34	Xmin = 302290 Xmax = 360880 Ymin = 6050800 Ymax = 6082300					
	Normalized number of points falling within depth range					
	Training dataset			Validation dataset		
Depth range [m]	Min	Median	Max	Min	Median	Max
<2	16.2%	16.5%	16.8%	16.3%	16.8%	17.7%
2–4	15.8%	16.1%	16.3%	15.3%	15.8%	16.4%
4–6	14.0%	14.5%	14.7%	13.3%	13.9%	14.9%
6–8	13.6%	13.8%	14.2%	12.8%	13.7%	14.2%
8–10	11.2%	11.4%	11.6%	11.0%	11.5%	12.0%
10–12	10.3%	10.6%	10.9%	9.9%	10.7%	11.3%
12–14	8.1%	8.3%	8.6%	7.7%	8.4%	8.8%
14–16	4.8%	5.1%	5.4%	4.5%	5.3%	6.1%
>16	3.7%	3.8%	4.0%	3.5%	3.8%	4.1%

ranges from 14% to 14.7% in the case of TD and from 13.3% to 14.9% for VD. Analogically, the fraction of points falling within the 6–8 m depth range, ranges from 13.6% to 14.2% (of TD) and 12.8–14.2% (of VD). A similar trend may be observed for other depth ranges. The higher variations for VD are caused by the smaller number of points than for TD (1017 and 2571 respectively). It is also important to notice that in the case of both datasets, the largest number of points, that the model used for training and verification, falls in the range between 2 and 12 meters (from 64.9% to 67.7% of VD and from 62.2% to 68.8% of TD), as this was the depth range that was primarily of interest in the case of this study.

Results and discussion

Following the methodology described in Eqs. 1–11, locally adjusted calibration and verification of the model was performed. The localization of centers of local sub-models (geographical and depth related) were constant for the whole study. In order to determine the center position of each local geographic model, at the first step, sounding transects were ordered in an eastward direction. Then, the whole dataset was divided into ten-element groups of adjacent transects and the geometrical middle of each group was considered to be the local model center. In the case presented, the proposed approach constitutes 12 local geographical models situated along the south Baltic coast and the northern part of the Hel Peninsula (Figure 4). Generally, in this case, an increase in the number of local sub-models would be desirable, as generally this would allow the method to better account for the spatial non-stationary aspect of the model. However, this approach is limited by the density and the number of available calibration points and in extreme cases, too many local sub-models may obscure general model performance

All calculations were performed in the native cartographic coordinate system, as applied to the Sentinel-2 observations (UTM 34N). In the next step, for every pixel of the satellite observation, geographical weight values, calculated from Eqs. 7,8, were assigned.

A similar methodology was applied to determine the depth related window centers. In this case, three static windows centered at 3, 8.25 and 13.75 [m] with assigned weights as presented in Figure 5, were assumed.

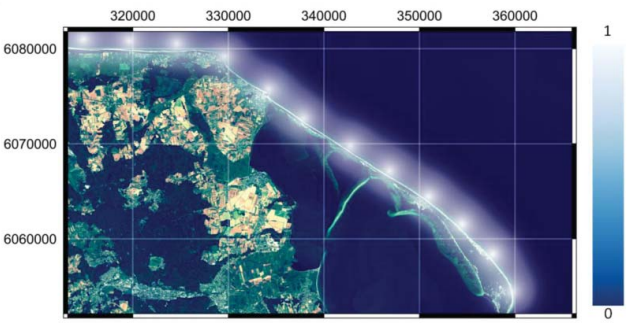

Figure 4. The position of the local model weighted location centers and geographical local model weights.

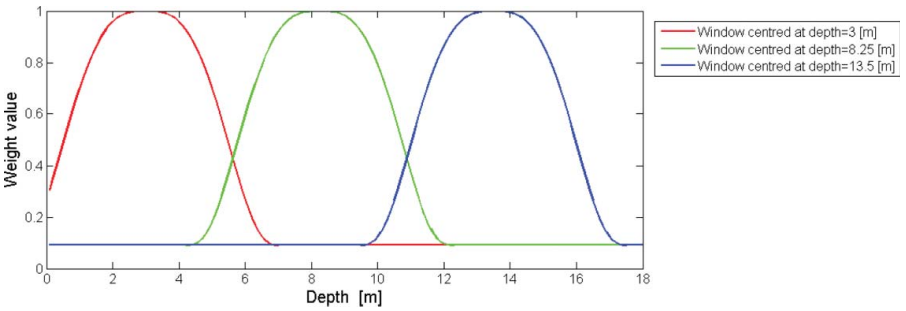

Figure 5. Depth windowing used for local depth dependent models.

Model calibration

The general color-coded overview of the product obtained with the use of the proposed SDB model acquired from selected observations is presented in Figure 6. The light blue color represents shallow depths and the dark blue depth represents areas with an estimated depth of up to 15 m. The background base map is constructed from true-color images on the basis of Sentinel-2 optical bands.

For each of the observations, the results obtained from the model training are presented in Table 3. In all cases, a strong correlation (R) between SDB and the training dataset ranges from 0.92–0.93 (in the case of an observation acquired on 4th March 2016) to 0.95–0.96 (in the case of an observation acquired on 6th May 2016), may be observed. Moreover, the general difference between the results obtained in individual iterations is relatively small, this confirms the hypothesis stated earlier, that the process of model training is relatively stable. Errors (RMSE) obtained during the proposed 3GWR model calibration range from 0.9 to 1.15 [m], and the differences between individual iterations and observations are noticeable but relatively small. Additionally, the comparison of results obtained by the proposed 3GWR model with the standard GWR approach, indicated the important conclusion that the proposed approach allows for a significant RMSE reduction (shown in the last column of Table 3) that ranges from 17% to 29% depending on the test case.

An additional analysis of error distribution, presented in Figure 7., shows a small positive bias ($\approx 0.5\ [m]$ depending on the observation) of residual errors which indicates that depths from remote observations are, to a small extent, under-estimated. Although its value is generally lower than the overall RMSE ($\approx 1\ [m]$), the general tendency of SDB underestimation may be observed. This is most probably caused by two factors. Firstly, in shallow areas (depths <4 m) the specular effects caused by wave foaming and sun glint from the non-flat sea surface is more noticeable. Moreover, wave foam affects the spectral content of the image, altering the reflectance intensity over the whole optical spectrum and this produces the result that more energy is registered by the sensor, as it would be for shallower pixels. The second reason is the difficulty in distinguishing between deep pixels for which a very small amount of light is reflected from the bottom, from those that are optically fully deep. In the results, there are some fully deep water pixels lying in the edge of these regions that are falsely indicated as a valid bathymetry estimation while the real depth exceeds the possibilities of remote estimation.

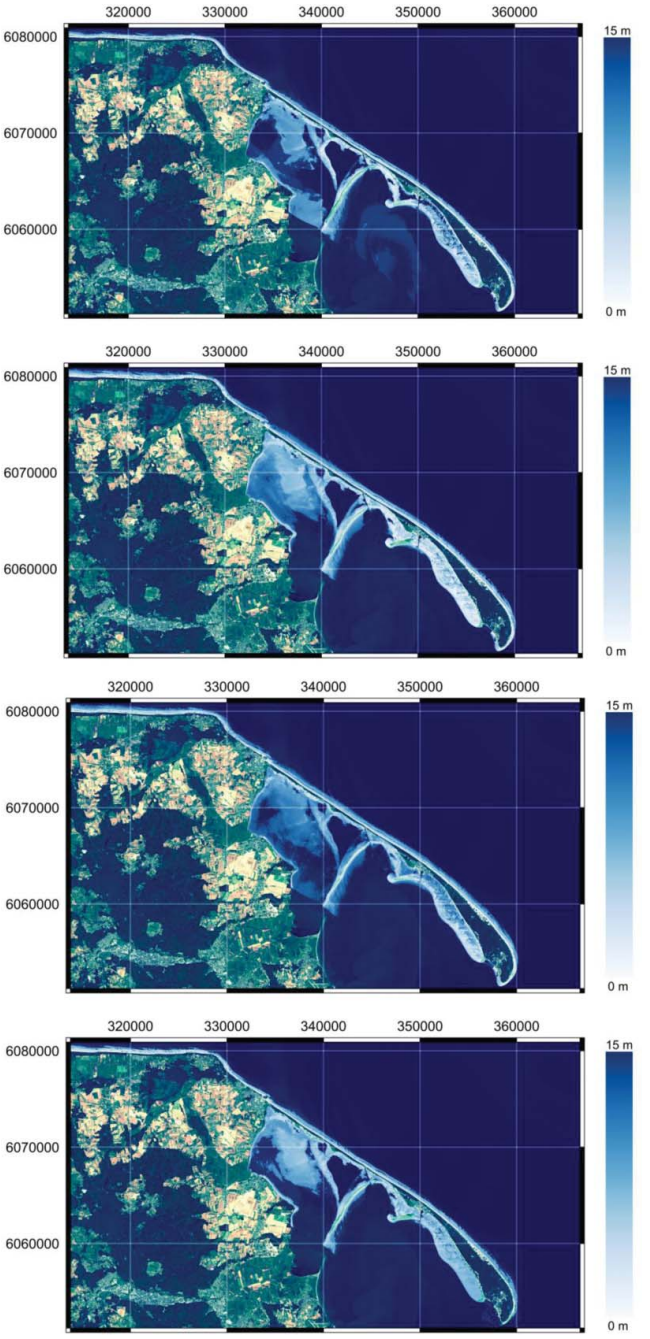

Figure 6. General overview of satellite derived bathymetry obtained by the proposed model from Sentinel-2 images registered on 4th March 2016 (upper picture), 9th March, 27th March and 6th May 2016 (lower pictures respectively) over the northern part of the Gulf of Gdańsk test site.

Table 3. Statistical results of model calibration obtained by the proposed SDB model. The results represent the results obtained only with the use of the training dataset. The procedure of model calibration was repeated 10 times.

Dataset/ Acquisition date	Proposed 3GWR		Standard GWR model		RMSE reduction (averaged) using 3GWR
	R (min-max)	RMSE [m] (min-max)	R (min-max)	RMSE [m] (min-max)	
4rd March 2016	0.92–0.93	1.1–1.15	0.9–0.91	1.34–1.38	17%
9th March 2016	0.95 ± 0.003	0.90–0.93	0.94	1.16–1.19	22%
27th March 2016	0.93–0.94	1.03–1.07	0.92 ± 0.03	1.45–1.48	28%
6th May 2016	0.95–0.96	1.11–1.13	0.94	1.56–1.6	29%

The presented results also indicate a relatively small variation in the residual error distribution as 50% of the results are within the − 0.5 to 1.5 m absolute error range, with extreme values of errors (3 and 97 percentile) slightly exceeding 3m. A more detailed analysis of the obtained results (not shown in the tables) also reveals that for every observation, over 90% of in situ verified points were characterized by an RMSE lower than the 2 [m] threshold and between 63.6% to 77% (depending on the observation) had an RMSE lower than 1m.

In Figure 8., the relationship between the obtained RMSE and the depth of points for each of the observations is presented. In this case, each figure shows the results of ten iterations of the training scheme and it may be observed, that for most of the depths, the RMSE obtained is lower than 1 [m]. Also note, that the errors obtained for shallower depths (<2 m) are higher than those for 8m depths. There are at least two reasons for that: firstly, in shallow water depths, wave break foaming effects have a significant influence on the optical properties of the surface of the water and thus generally disturb the model learning process. Secondly, the much higher spatial diversity of shallow water optical properties may be expected due to the presence of sediment and particles in the water. On the other hand, the lowest errors were observed for depths of around 8m, this may be caused by the fact, that the local depth window center is placed in this value. For depths of over 10m, a significant increase in

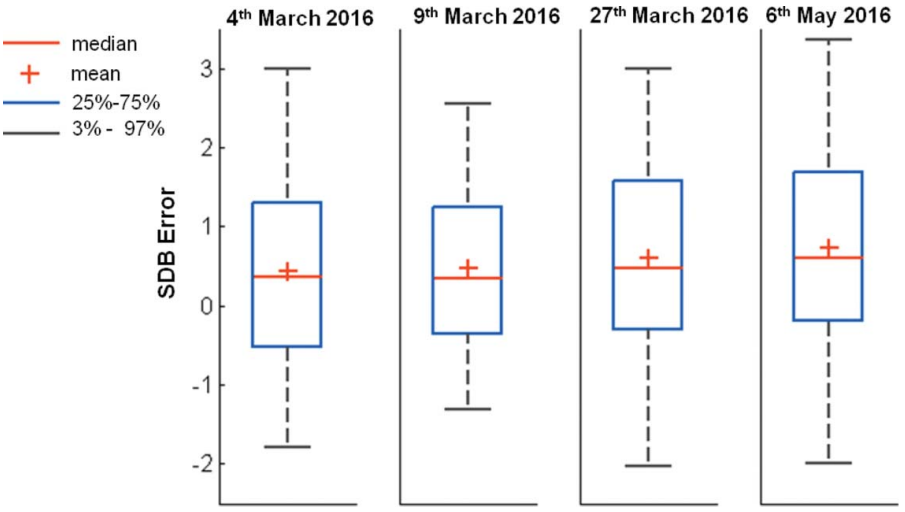

Figure 7. Boxplots of the statistical distribution of the satellite derived bathymetry residual error (difference between SBE sounding and SDB) accumulated from all iterations of model training.

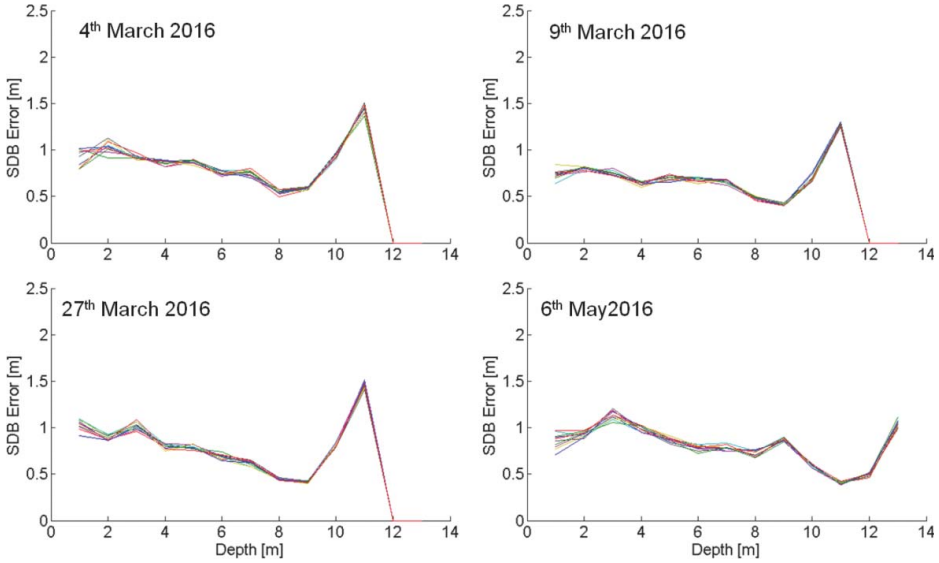

Figure 8. Depth related RMSE obtained during the model calibration process. Each of the figures represents the results of 10 iterations of the model training process.

RMSE may be observed, as this is probably close to the limit of maximal depth derivation for the analyzed test site.

Model verification

In order to evaluate the proposed model performance, we compared the results obtained by a trained SDB model to the external data – validation dataset (Table 4). It may be observed, that the results of model verification show a strong similarity to those obtained when using a training set. This means that the model performance is satisfactory when external data, that was not used for model training, is utilized. The correlation coefficient error obtained is negligibly smaller than is the case for the model training process and in all cases exceeds 0.9, namely from 0.91 (in the case of an observation acquired on 4th March 2016) to 0.95 (in the case of an observation acquired on 9th March and 6th May 2016). Similar conclusions may be drawn regarding the obtained RMSE calculated on the basis of the validation dataset. In particular, errors were obtained from the use of a calibrated model tested with a validation

Table 4. Statistical results of model verification obtained by the proposed calibrated SDB model. The table represents the results obtained with the use of validation dataset only. The procedure of model verification was repeated 10 times.

Dataset/ Acquisition date	Proposed 3DGWR		Standard GWR model		RMSE reduction (averaged) using 3GWR
	R (min-max)	RMSE [m] (min-max)	R (min-max)	RMSE [m] (min-max)	
4rd March 2016,	0.91–0.93	1.07–1.23	0.9–0.91	1.31–1.46	17%
9th March 2016,	0.95±0.005	0.88–0.95	0.94	1.16–1.24	23%
27th March 2016	0.93–0.94	1.01–1.07	0.91–0.92	1.45–1.5	29%
6th May 2016	0.95±0.004	1.08–1.14	0.93–0.94	1.53–1.62	30%

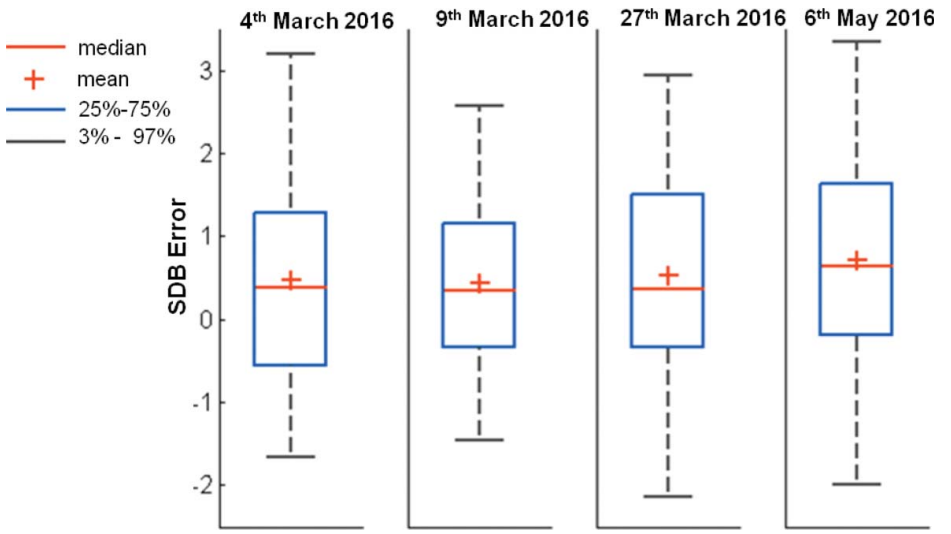

Figure 9. Boxplot statistical analysis of the residual errors of the proposed SDB data verified on validation dataset soundings.

dataset range from 0.88 [m] to 1.23 [m]. Moreover, variations between iterations for each observation, do not exceed 0.16 m (most variation was observed in the case of an observation acquired on 4th March 2016). The proposed 3DGWR approach was also compared with the GWR model in terms of basic statistical measurements. In this case, it may be observed that the application of the proposed approach significantly improves the overall model performance in comparison to the standard GWR technique which, as a consequence, allows for RMSE reduction from 17% to 30%.

An additional statistical analysis of error distribution, analogous to the TD case, is presented in Figure 9. It clearly shows, that error distribution in the case of model validation is very similar to the results obtained when using training data. Presented in the form of boxplots, residual error analysis indicates a relatively small variation of errors and a similar ($\approx 0.5\,m$) bias, which also, in this case, indicates a small under-estimation of bathymetry when using remote observations. Additional calculations, also show that, in the case of validation data, the estimated bathymetry of over 63% of sounding points was characterized by an RMSE lower than 1 [m] and for over 92% of VD points the RMSE of remote bathymetry estimation was lower than the 2m threshold.

An analogous analysis of RMSE dependence in relation to the depth of sounding in VD was presented in Figure 10. It may be observed, that similarly, as in the case of the training data (Figure 6), RMSE shows no special dependence due to the depth of the observed pixel in the range of 2–10m, which is the result of a good model fit to local depth related to the conditions of approximated data. With regard to extreme error values, in this case, the smallest RMSE error was obtained for depths of 8–9 meters. Similarly, as in the TD case, there might be at least two reasons for that: firstly, for depths of over 6m the amount of sediment and particles in the water column is relatively less observable than for shallow water and therefore the water attenuation coefficient is more stable over the analyzed area. Secondly, the lowest RMSE at this depth range is also probably caused by the fact that it is near the depth dependent window center (Figure 4).

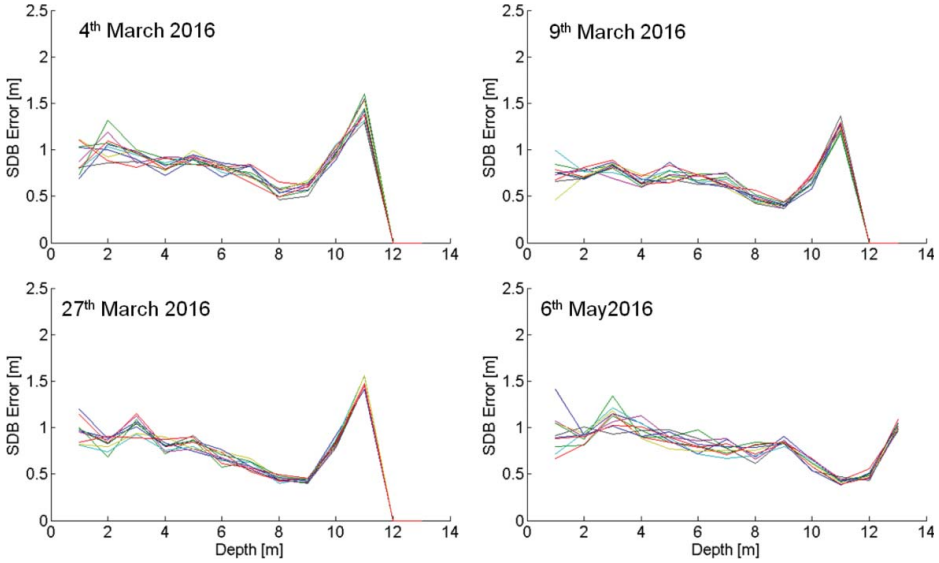

Figure 10. Results of model validation.

With regard to the general conclusions concerning the obtained RMSE in comparison to results obtained in different studies, it should be stated that, there are at least two factors that have a negative influence on the final proposed model performance. The first thing is the difference between the time that the in situ data was acquired and the time that the remote observations were registered. In case of this study, TD and VD surveys were made from 1 to 5 years earlier than the observations and, during this time, significant changes in bathymetry in the observed area may have taken place. The second factor, is the spatial resolution of observations that cannot capture bathymetry variations within the area of one pixel.

Application of the algorithm

In order to verify whether the proposed 3GWR SDB model may be used outside the calibration site, an analysis of SDB obtained by the proposed approach for areas in the vicinity of Jastarnia port (54°41′46.2″N 18°40′30.5″E), that is placed in the middle of the south coast of Hel Peninsula, was performed. It is worth mentioning that the vicinity of Jastarnia port is not part of the calibration test site of the model, as it is situated on the other (southern) coast of Hel Peninsula. However, an analysis of this test-case is important, because it covers important marine route for numerous touristic vessels and fishing boats. This site is also unusual as most of this area has a sandy bottom and, therefore, this maritime route needs to be frequently monitored in order ensure maritime traffic safety.

In Figure 11 two consecutive SDB observations made on 4th March and 6th May of 2016 (Figure 8) with depths ranging from close to 0 m up to 20 m are presented. It may be observed that the route consists of an approximately 150m wide passage placed between two shallow water fields and its maximal depth exceeds 7m.

Transects indicated on the observations registered on 4th March 2016 (points A, B, C and D) and 6th May 2016 (corresponding points A′, B′, C′ and D′) were defined in order to present the usefulness of the proposed model in observing the process of sediment migration in

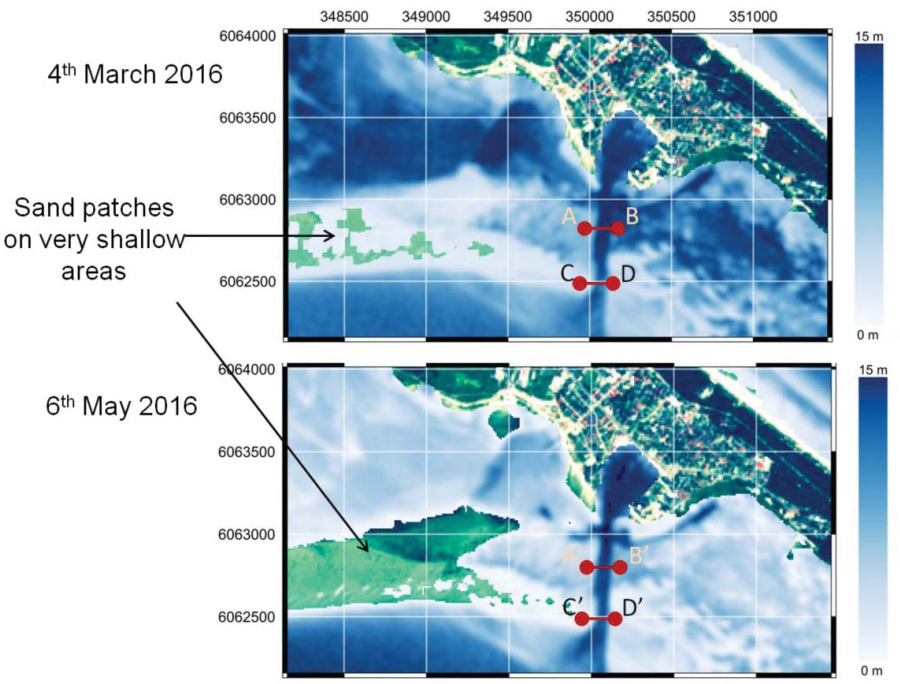

Figure 11. Satellite derived bathymetry of the area in the vicinity of Jastarnia Port, the middle part of the southern coast of Hel Peninsula. Two derived bathymetry maps were obtained with the use of the proposed 3GWR model from observations acquired on 4th March and 6th May of 2016. Manually fixed points (ABCD and A′B′C′D) indicate transverse transects (red lines in the figure) of the marine route. Data is presented in the UTM 34N coordinate system.

this area. Namely, in Figure 12, depths along transects were extracted in order to show temporal changes of bathymetry within the analyzed maritime route. The presented results, clearly show the process of the flattening of the sea route in the vicinity of the port, which is the result of sediment migration along the southern part of Hel peninsula.

Namely, according to the proposed SDB model, in the case of the AB (A′B′) transect, it may be observed that the depth of point A (A′) has decreased from 3.75 m to 1.9 m during the period from March to May. An even bigger difference may be observed for point B (B′), where the depth decreased almost 4 m (from 8 m to 4.1 m). The depth of the transects, in its middle part, is similar (total depth of approximately 8–8.5 m and the difference between observations is relatively small – about 20–30 cm), which confirms the conclusion, that both SDB observations, though registered in different periods, may be used to monitor temporal changes of bathymetry. An analogous conclusion may be drawn for the CD (C′D′) transect, as the observable depth decreases, in this case, for both points, by ≈1 m, with the middle of the transect showing no noticeable difference. This issue also confirms the hypothesis stated earlier, regarding errors produced by the model. Namely, errors in bathymetry estimation are more likely to be the result of the low spatial resolution of remote observations rather than just the inaccuracy of the model itself. This is because, the variations of bathymetry within the area of one pixel ($10\,m.\ \times\ 10\,m.$), cannot be captured by remote observation and thus the model is not capable of fitting to the local distortions of bathymetry. Moreover, the comparison of corresponding pixels in different observations rather suggests that the model

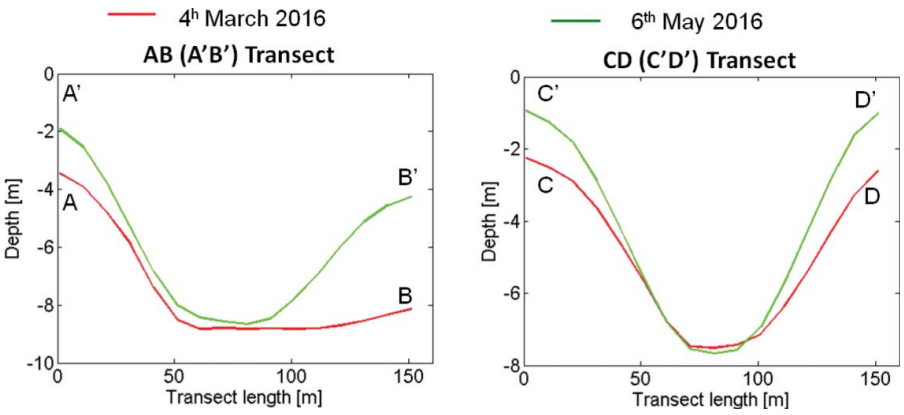

Figure 12. Comparison of SDB profiles between 4th March and 6th May of 2016.The figure shows a significant difference in the depth of points that are bound the maritime route.

is capable of acquiring a higher level of precision because the depths of transects in their middle part remain static between observations as observed changes in bathymetry estimation were less than 0.5 m.

Conclusions

In this paper, the proposed original 3-dimensional geographical weighted regression (3GWR) method for satellite bathymetry derivation (SDB) based on multiple local regression models was presented. The novelty of the proposed approach relies on the fact, that the presented technique binds together previously known models from the literature, namely geographical weighted regression models (GWR), with local depth related inverse regression optimization, which is used to derive the best possible (in the sense of the mean square error) bathymetry model. The data for model training and its verification was acquired by a single beam echosounder and provided by the Polish Maritime Administration.

The Author of the paper conducted experiments in relatively difficult SDB model areas, which are characterized by a high level of sediment and lower water clarity than other typical test sites presented in different studies. Nevertheless, it was shown, that the proposed technique is useful at a global and local scale, to depths up to 12 meters. The results presented in this paper, indicate that the proposed SDB model allows for an estimation of bathymetry in near shore areas with errors ranging from $RMSE = 0.88$ [m] to $RMSE = 1.23$ $[m]$ and a high correlation ranging from 0.91 to 0.95 depending on the observation. The variation in the residual errors of the proposed approach are relatively small as 50% of the results fall in the -0.5 to 1.5 m error range with a bias of $\approx$0.5 m and bathymetry of over 60% of the points of the validation dataset were estimated to have a RMSE lower than 1m.

The results of the proposed approach were also verified during the conducted practical use-case experiment, where the proposed method for SDB estimation was used to assess the changes of the bottom of the maritime route near the observed test site. The presented results indicate a high application potential for the proposed methods with regard to activities related to assessing the changes in bathymetry of near shore areas. This is particularly

important for locations where temporal bathymetry rapidly changes, for instance due to sand migration, and therefore the area must be continuously monitored in order to ensure the safety of marine routes. The proposed model was tested and verified for a particular maritime route, namely the route to the Jastarnia Port placed in the middle of the south coast of the Hel Peninsula, Poland.

The study presented in this paper shows that the proposed SDB model, though tested in difficult conditions, is capable of extracting the temporal changes in the near shore bathymetry and, in consequence, can generally increase the level of maritime traffic safety.

Acknowledgments

The author wishes to thank the Maritime Office in Gdynia, Poland for providing survey sounding bathymetry data used during the research presented in the paper.

References

Allen, J. G., N. B. Nelson, and D. A. Siegel. 2017. Seasonal to multi-decadal trends in apparent optical properties in the Sargasso sea. *Deep-Sea Research Part I-Oceanographic Research Papers* 119(January):58–67. doi:10.1016/j.dsr.2016.11.004

Bramante, J. F., D. K. Raju, and T. M. Sin. 2013. Multispectral derivation of bathymetry in Singapore's shallow, turbid waters. *International Journal of Remote Sensing* 34(6):2070–88. doi:10.1080/01431161.2012.734934

Brando, V. E., and A. G. Dekker. 2003. Satellite hyperspectral remote sensing for estimating estuarine and coastal water quality. *IEEE Transactions on Geoscience and Remote Sensing* 41(6):1378–87. doi:10.1109/TGRS.2003.812907

Brando, V. E., J. M. Anstee, M. Wettle, A. G. Dekker, S. R. Phinn, and C. Roelfsema. 2009. A physics based retrieval and quality assessment of bathymetry from suboptimal hyperspectral data. *Remote Sensing of Environment* 113(4):755–70. doi:10.1016/j.rse.2008.12.003

Chavez Jr., P. S. 1996. Image-based atmospheric corrections revisited and improved. *Photogrammetric Engineering & Remote Sensing* 62(9):1025–36.

Cleveland, W. S., and S. J. Devlin. 1988. Locally weighted regression – an approach to regression-analysis by local fitting. *Journal of the American Statistical Association* 83(403):596–610. doi:10.2307/2289282

Corucci, L., A. Masini, and M. Cococcioni. 2011. Approaching bathymetry estimation from high resolution multispectral satellite images using a neuro-fuzzy technique. *Journal of Applied Remote Sensing* 5(1):053515–053515-15. doi:10.1117/1.3569125

Doernhoefer, K., A. Goeritz, P. Gege, B. Pflug, and N. Oppelt. 2016. Water constituents and water depth retrieval from Sentinel-2A-A first evaluation in an oligotrophic lake. *Remote Sensing* 8(11):941. doi:10.3390/rs8110941

Eugenio, F., J. Marcello, and J. Martin. 2015. High-resolution maps of bathymetry and benthic habitats in shallow-water environments using multispectral remote sensing imagery. *IEEE Transactions on Geoscience and Remote Sensing* 53(7):3539–49. doi:10.1109/TGRS.2014.2377300

Forfinski-Sarkozi, N. A., and C. E. Parrish. 2016. Analysis of MABEL bathymetry in Keweenaw Bay and implications for ICESat-2 ATLAS. *Remote Sensing* 8(9):772. doi:10.3390/rs8090772

Fotheringham, A. S., M. E. Charlton, and C. Brunsdon. 1998. Geographically weighted regression: a natural evolution of the expansion method for spatial data analysis. *Environment and Planning A* 30(11):1905–27. doi:10.1068/a301905

Giardino, C., G. Candiani, M. Bresciani, Z. Lee, S. Gagliano, and M. Pepe. 2012. BOMBER: A tool for estimating water quality and bottom properties from remote sensing images. *Computers & Geosciences* 45(August):313–18. doi:10.1016/j.cageo.2011.11.022

Guzinski, R., E. Spondylis, M. Michalis, S. Tusa, G. Brancato, L. Minno, and L. B. Hansen. 2016. Exploring the utility of bathymetry maps derived with multispectral satellite observations in the field of underwater archaeology. *Open Archaeology* 2(1):243–263. doi:10.1515/opar-2016-0018.

Hamylton, S. M., J. D. Hedley, and R. J. Beaman. 2015. Derivation of high-resolution bathymetry from multispectral satellite imagery: a comparison of empirical and optimisation methods through geographical error analysis. *Remote Sensing* 7(12):16257–73. doi:10.3390/rs71215829

Harborne, A. R., and P. J. Mumby. 2005. Technical note: Simple and robust removal of sun glint for mapping shallow-water benthos. *International Journal of Remote Sensing* 26(10):2107–12. doi:10.1080/01431160500034086.

Hedley, J., C. Roelfsema, B. Koetz, and S. Phinn. 2012. Capability of the Sentinel-2 mission for tropical coral reef mapping and coral bleaching detection. *Remote Sensing of Environment The Sentinel Missions – New Opportunities for Science* 120(May):145–55. doi:10.1016/j.rse.2011.06.028

Hoge, F. E., and P. E. Lyon. 1996. Satellite retrieval of inherent optical properties by linear matrix inversion of oceanic radiance models: an analysis of model and radiance measurement errors. *Journal of Geophysical Research: Oceans* 101(C7):16631–48. doi:10.1029/96JC01414

Jena, B., P. J. Kurian, D. Swain, A. Tyagi, and R. Ravindra. 2012. Prediction of bathymetry from satellite altimeter based gravity in the Arabian sea: mapping of two unnamed deep seamounts. *International Journal of Applied Earth Observation and Geoinformation* 16(June):1–4. doi:10.1016/j.jag.2011.11.008

Kanno, A., Y. Koibuchi, and M. Isobe. 2011. Statistical combination of spatial interpolation and multispectral remote sensing for shallow water bathymetry. *Ieee Geoscience and Remote Sensing Letters* 8 (1):64–67. doi:10.1109/LGRS.2010.2051658

Kay, S., J. D. Hedley, and S. Lavender. 2009. Sun glint correction of high and low spatial resolution images of aquatic scenes: A review of methods for visible and near-infrared wavelengths. *Remote Sensing* 1(4):697–730. doi:10.3390/rs1040697

Knudby, A., S. K. Ahmad, and C. Ilori. 2016. The potential for landsat-based bathymetry in Canada. *Canadian Journal of Remote Sensing* 42(4):367–78. doi:10.1080/07038992.2016.1177452

Kobryn, H. T., K. Wouters, L. E. Beckley, and T. Heege. 2013. Ningaloo reef: shallow marine habitats mapped using a hyperspectral sensor. *Plos One* 8(7):e70105. doi:10.1371/journal.pone.0070105

Kulawiak, M., A. Chybicki, and M. Moszynski. 2010. Web-based GIS as a tool for supporting marine research. *Marine Geodesy* 33(2,3):135–53. doi:10.1080/01490419.2010.492280

Kyriakidis, I., K. Karatzas, A. Ware, and G. Papadourakis. 2016. A generic preprocessing optimization methodology when predicting time-series data. *International Journal of Computational Intelligence Systems* 9(4):638–51. doi:10.1080/18756891.2016.1204113

Lafon, V., J. M. Froidefond, F. Lahet, and P. Castaing. 2002. SPOT shallow water bathymetry of a moderately turbid tidal inlet based on field measurements. *Remote Sensing of Environment* 81 (1):136–48. doi:10.1016/S0034-4257(01)00340-6

Lee, K. R., R. C. Olsen, and F. A. Kruse. 2012. Using multi-angle worldview-2 imagery to determine ocean depth near the island of Oahu, Hawaii. In *Algorithms and Technologies for Multispectral, Hyperspectral, and Ultraspectral Imagery XVIII*. Shen S. S. and Lewis P. E. (eds.), vol. 8390, 83901I. Bellingham: Spie-Int Soc Optical Engineering.

Lee, Z., K. L. Carder, C. D. Mobley, R. G. Steward, and J. S. Patch. 1998. Hyperspectral remote sensing for shallow waters. I. A semianalytical model. *Applied Optics* 37(27):6329–38.

Liu, Z. 2013. Bathymetry and bottom albedo retrieval using Hyperion: a case study of Thitu Island and reef. *Chinese Journal of Oceanology and Limnology* 31(6):1350–55. doi:10.1007/s00343-013-2287-8

Luchinin, A. G., and M. Y. Kirillin. 2016. Temporal and frequency characteristics of a narrow light beam in sea water. *Applied Optics* 55(27):7756–62. doi:10.1364/AO.55.007756

Lyzenga, D. R. 1981. Remote sensing of bottom reflectance and water attenuation parameters in shallow water using aircraft and landsat data. *International Journal of Remote Sensing* 1, 2(1):71–82.

Lyzenga, D. R., N. P. Malinas, and F. J. Tanis. 2006. Multispectral bathymetry using a simple physically based algorithm. *IEEE Transactions on Geoscience and Remote Sensing* 44(8):2251–59. doi:10.1109/TGRS.2006.872909

Lyzenga, D. R. 1977. Reflectance of a flat ocean in limit of zero water depth. *Applied Optics* 16(2):282–83. doi:10.1364/AO.16.000282

Ma, S., Z. Tao, X. Yang, Y. Yu, X. Zhou, and Z. Li. 2014. Bathymetry retrieval from hyperspectral remote sensing data in optical-shallow water. *IEEE Transactions on Geoscience and Remote Sensing* 52(2):1205–12. doi:10.1109/TGRS.2013.2248372

Mahiny, A. S., and B. J. Turner. 2007. A comparison of four common atmospheric correction methods. *Photogrammetric Engineering & Remote Sensing* 73(4):361–68. doi:10.14358/PERS.73.4.361

Martins, V. S., C. C. F. Barbosa, L. A. S. de Carvalho, D. S. F. Jorge, F. de Lucia Lobo, and E. M. L. de Moraes Novo. 2017. Assessment of atmospheric correction methods for Sentinel-2 MSI images applied to amazon floodplain lakes. *Remote Sensing* 9(4):322. doi:10.3390/rs9040322

Mishra, D. R., S. Narumalani, D. Rundquist, and M. Lawson. 2005. High-resolution ocean color remote sensing of benthic habitats: a case study at the Roatan Island, Honduras. *IEEE Transactions on Geoscience and Remote Sensing* 43(7):1592–1604. doi:10.1109/TGRS.2005.847790

Mishra, D., S. Narumalani, D. Rundquist, and M. Lawson. 2006. Benthic habitat mapping in tropical marine environments using quickbird multispectral data. *Photogrammetric Engineering & Remote Sensing* 72(9):1037–1048.

Mishra, D. R., S. Narumalani, D. Rundquist, M. Lawson, and R. Perk. 2007. Enhancing the detection and classification of coral reef and associated benthic habitats: a hyperspectral remote sensing approach. *Journal of Geophysical Research: Oceans* 112:C08014. doi:10.1029/2006JC003892

Mobley, C. D., L. K. Sundman, C. O. Davis, J. H. Bowles, T. V. Downes, R. A. Leathers, M. J. Montes, et al. 2005. Interpretation of hyperspectral remote-sensing imagery by spectrum matching and look-up tables. *Applied Optics* 44(17):3576–92. doi:10.1364/AO.44.003576

Moszynski, M., M. Kulawiak, A. Chybicki, K. Bruniecki, T. Bielinski, Z. Lubniewski, and A. Stepnowski. 2015. Innovative web-based geographic information system for municipal areas and coastal zone security and threat monitoring using EO satellite data. *Marine Geodesy* 38(3):203–24. doi:10.1080/01490419.2014.969459

Moussavi, M. S., W. Abdalati, A. Pope, T. Scambos, M. Tedesco, M. MacFerrin, and S. Grigsby. 2016. Derivation and validation of supraglacial lake volumes on the Greenland ice sheet from high-resolution satellite imagery. *Remote Sensing of Environment* 183(September):294–303. doi:10.1016/j.rse.2016.05.024

Pacheco, A, A. Horta, J. O. Loureiro, and O. Ferreira. 2015. Retrieval of nearshore bathymetry from landsat 8 images: a tool for coastal monitoring in shallow waters. *Remote Sensing of Environment* 159(0):102–16.

Pe'eri, S., C. Parrish, C. Azuike, L. Alexander, and A. Armstrong. 2014. Satellite remote sensing as a reconnaissance tool for assessing nautical chart adequacy and completeness. *Marine Geodesy* 37 (3):293–314. doi:10.1080/01490419.2014.902880

Pope, A., T. A. Scambos, M. Moussavi, M. Tedesco, M. Willis, D. Shean, and S. Grigsby. 2016. Estimating supraglacial lake depth in west Greenland using landsat 8 and comparison with other multispectral methods. *Cryosphere* 10(1):15–27. doi:10.5194/tc-10-15-2016

Pope, R. M., and E. S. Fry. 1997. Absorption spectrum (380–700 Nm) of pure water. II. Integrating cavity measurements. *Applied Optics* 36(33):8710–23. doi:10.1364/AO.36.008710

Spitzer, D, and R.W. J. Dirks. 1986. Shallow water bathymetry and bottom classification by means of the Landsat and SPOT optical scanners. *1986 International Symposium/Innsbruck* 0660:136–38. doi:10.1117/12.938578.

Stulp, F., and O. Sigaud. 2015. Many regression algorithms, one unified model: a review. *Neural Networks* 69(September):60–79. doi:10.1016/j.neunet.2015.05.005

Stumpf, R. P., K. Holderied, and M. Sinclair. 2003. Determination of water depth with high-resolution satellite imagery over variable bottom types. *Limnology and Oceanography* 48(1part2):547–56. doi:10.4319/lo.2003.48.1_part_2.0547

Su, H., H. Liu, L. Wang, A. M. Filippi, W. D. Heyman, and R. A. Beck. 2014. Geographically adaptive inversion model for improving bathymetric retrieval from satellite multispectral imagery. *IEEE Transactions on Geoscience and Remote Sensing* 52(1):465–76. doi:10.1109/TGRS.2013.2241772

Su, H., H. Liu, and Q. Wu. 2015. Prediction of water depth from multispectral satellite imagery #x2014; The regression kriging alternative. *IEEE Geoscience and Remote Sensing Letters* 12 (12):2511–15. doi:10.1109/LGRS.2015.2489678

Su, H., H. Liu, and W. D. Heyman. 2008. Automated derivation of bathymetric information from multi-spectral satellite imagery using a non-linear inversion model. *Marine Geodesy* 31(4):281–98. doi:10.1080/01490410802466652

Toming, K., T. Kutser, A. Laas, M. Sepp, B. Paavel, and T. Nõges. 2016. First experiences in mapping lake water quality parameters with Sentinel-2 MSI imagery. *Remote Sensing* 8(8):640. doi:10.3390/rs8080640

Vahtmäe, E., T. Kutser, G. Martin, and J. Kotta. 2006. Feasibility of hyperspectral remote sensing for mapping benthic macroalgal cover in turbid coastal waters—a Baltic sea case study. *Remote Sensing of Environment* 101(3):342–51. doi:10.1016/j.rse.2006.01.009

Vahtmaee, E., and T. Kutser. 2016. Airborne mapping of shallow water bathymetry in the optically complex waters of the Baltic sea. *Journal of Applied Remote Sensing* 10(May):025012. doi:10.1117/1.JRS.10.025012

Vinayaraj, P., V. Raghavan, S. Masumoto, and J. Glejin. 2015. Comparative evaluation and refinement of algorithm for water depth estimation using medium resolution remote sensing data. *International Journal of Geoinformatics* 11(3):17–29.

Vinayaraj, P., V. Raghavan, and S. Masumoto. 2016. Satellite-derived bathymetry using adaptive geographically weighted regression model. *Marine Geodesy* 39(6):458–78. doi:10.1080/01490419.2016.1245227

Wieczorek, M. M., W. A. Spallek, T. Niedzielski, J. A. Godbold, and I. G. Priede. 2014. Use of remotely-derived bathymetry for modelling biomass in marine environments. *Pure and Applied Geophysics* 171(6):1029–45. doi:10.1007/s00024-013-0705-7